Quantum, Statistical and Quasiclassical Trajectory Studies For The Ne + $HeH^+ \rightarrow NeH^+$ + He Reaction On The Ground Electronic State

Debasish Koner,[†] Lizandra Barrios,[‡] Tomás González-Lezana,[*,‡] and Aditya N. Panda[*,†]

Department of Chemistry, Indian Institute of Technology Guwahati, 781039, India, and Instituto de Física Fundamental, C.S.I.C., Serrano 123, Madrid 28006, Spain

E-mail: t.gonzalez.lezana@csic.es; adi07@iitg.ernet.in

Abstract

Real wave packet, statistical quantum and quasiclassical trajectory methods have been employed to study the dynamics of Ne + $HeH^+(v_0, j_0) \rightarrow$ He + NeH^+ reaction on an ab initio potential energy surface [*J. Phys. Chem. A* **2013**, *117, 13070-13078*]. Quantum and statistical quantum calculations have been performed within the centrifugal sudden (CS) approximation as well as including the Coriolis coupling(CC). Dense oscillatory structures of the quantum reaction probabilities and fair agreement between quantum and statistical cross sections suggest a complex forming mechanism for the reaction. No significant differences between cross sections obtained within the CS and CC approaches are observed. Classical trajectory results give an excellent average description of the quantum CC results. At low collision energies, there is a substantial decrease in reactivity for the reaction upon rovibrational excitation. Initial state

[*]To whom correspondence should be addressed
[†]Department of Chemistry, Indian Institute of Technology Guwahati, 781039, India
[‡]Instituto de Física Fundamental, C.S.I.C., Serrano 123, Madrid 28006, Spain

selected rate constants for the title reaction are calculated between 20 K and 1000 K and the calculated value at 300 K agrees quite well with the available experimental result. Reaction cross sections and rate constants are also compared with those calculated via the Langevin capture model for exothermic reactions.

Introduction

Hydrogen and helium are the two most abundant components of the interstellar medium (ISM). Both are the results of primordial nucleosynthesis and form HeH^+,[1–3] the first molecular ionic system of the universe which plays an important role in various cosmological phenomena.[1,3,4] Other rare gases such as neon and argon are also present in a considerable amount in the ISM.[5–8] Recently ArH^+ molecular ion has been detected in Crab nebula from spectra recorded by the Herschel Space Observatory.[6] Collisions between atoms of these rare gases and either H^+ or HeH^+ are thus possible in the ISM environment since most of these ion-molecule reactions possess no barriers and can take place at very low temperatures. Therefore, besides a fundamental relevance on the dynamics of such processes, their study can provide useful knowledge regarding the evolution of the ISM. Both theoretical and experimental recent advances in gas-phase ion chemistry of rare gases, as shown in the review article by F. Grandinetti,[9] reveals the interest in the subject.

Dynamics of reactions involving Ne and He (the two rare gases among the six most abundant elements in the Solar System[10]) and hydrogen molecular ion has been widely studied.[11–21] Involvement of only the ground electronic surface in the dynamics makes these reactions easier for studying. This type of proton transfer processes usually follow a complex-forming mechanism due to the presence of potential energy minima along the reaction path and this results in numerous resonances in the corresponding probabilities. The exothermic $HeH^+ + H \rightarrow He + H_2^+$ reaction, which plays an important role in the early universe evolution scenario,[3,4] has been studied recently in ultracold to hyperthermal region via time independent quantum reactive scattering and time dependent (TD) real wave packet (RWP) methods, respectively by De Fazio[22] and Gamallo et. al.[23] The reaction was found to be less sensitive towards ro-vibrational excitation in the hyperthermal region. He_2H^+ system has been widely studied theoretically, which includes electronic structure calculation,[24] generation of ab initio potential energy surfaces (PES),[25,26] calculation of bound and quasibound states[25] and studying reactive scattering via time dependent quantum mechanical (TDQM) method.[27,28] We have recently investigated the $[HeHNe]^+$ system, a mixed rare gas cationic hydride. The electronic structural details for this system have been explored and it

is found that like other protonated rare gas systems, $[HeHNe]^+$ is most stable at linear (He-H-Ne) configuration.[29] In 1978, Matcha et al. constructed a collinear diatomic-in-molecules PES for the $[HeHNe]^+$ system.[30] Recently, a global analytic surface with a small root mean square error for this system has been constructed and preliminary quantum dynamical studies have been performed within centrifugal sudden (CS) approximation by some of us, for the endothermic He + NeH^+ $\rightarrow$ HeH^+ + Ne reaction.[31] Oscillatory behavior of the CS reaction probabilities suggests complex-forming mechanism as a plausible path for the reaction. Necessity of inclusion of Coriolis coupling (CC) to study bimolecular complex forming reactions has been discussed in the literature.[14,28,32–37] In our recent article,[37] we reported the results of reactive scattering studies for the above reaction for different rovibrational reactant states via RWP and statistical quantum mechanical (SQM) methods, within CS approximation as well as including Coriolis coupled states. Significant differences noticed between quantum CS and CC results highlighted the importance of a proper treatment of the helicity components coupling for this reaction. SQM results were in a fairly good agreement with the RWP results for the ground vibrational state. Vibrational excitation of the reactants was found to greatly enhance the reactivity of the reaction, while rotational excitation of the reactants resulted in inhibiting the process.

In this article, we report a detailed computational study for the reaction Ne + HeH^+ $\rightarrow$ NeH^+ + He. A schematic potential energy profile for the process is shown in Figure 1. Different rovibrational states of reactants and products are also presented in the same figure. As can be seen, the reactive process is barrierless and exothermic by 0.293 eV. The PES is characterized by a potential well which has a depth of $\sim$0.8 eV (with respect to the reactant asymptote) for $\widehat{NeHHe}$ = 180°, with values of the interparticle distances of r_{NeH} =2.102 bohr and r_{HeH} =1.804 bohr at the minimum configuration, which may trap the $[HeHNe]^+$ collision complex. Glosík et al.[38] have studied this reaction experimentally by using selected ion flow tube apparatus and the rate constant at 300 K has been reported to be $1.25 \pm 0.625 \times 10^{-9}$ cm^3 s^{-1}. To the best of our knowledge, this is the first theoretical study of the title reaction. RWP, SQM and quasiclassical trajectory (QCT) methods are employed to investigate the dynamics of the process for various rovibrational states of

the HeH^+ reactant. Both CS and CC reaction probabilities are computed from TDQM and SQM simulations. Comparisons between QM and QCT results are carried out to determine the extent of quantum effects on the observables.

This article is arranged as follows: Quantum, statistical and quasiclassical methodologies are discussed briefly in Sec. II. In Sec. III, results are presented and discussed. Concluding remarks are given in Sec. IV.

Methods

Real wave packet method

The RWP method followed here is discussed in detail in our previous article[37] and only a brief outline is presented here. The Hamiltonian operator for the Ne+HeH^+ system is expressed in reactant Jacobi coordinates as[39]

$$\hat{H} = -\frac{\hbar^2}{2\mu_R}\frac{\partial^2}{\partial R^2} - \frac{\hbar^2}{2\mu_r}\frac{\partial^2}{\partial r^2} + \frac{(\mathbf{J}-\mathbf{j})^2}{2\mu_R R^2} + \frac{\mathbf{j}^2}{2\mu_r r^2} + \mathbf{V}(R,r,\theta), \tag{1}$$

where R is the distance between Ne atom and the center of mass of HeH^+, r is the HeH^+ bond length, μ_R is the reduced mass of Ne and HeH^+ and μ_r is the reduced mass of HeH^+. $\mathbf{J}$ and $\mathbf{j}$ are the total angular momentum and rotational angular momentum operators, respectively. $\mathbf{V}(R,r,\theta)$ is the interaction potential of the system.

The wave packet (WP) propagation is carried out via a modified Chebyshev method:[40] $\Phi_{k+1} = D(2\hat{H}_s\Phi_k - D\Phi_{k-1})$, where $\hat{H}_s$ is the Hamiltonian of the system scaled to be within [-1,1]. $\hat{H}_s$ is expressed as $\hat{H}_s = (\hat{H} - H^+)/H^-$ with $H^+ = (H_{\max} + H_{\min})/2$ and $H^- = (H_{\max} - H_{\min})/2$. Here $H_{\max}$ and $H_{\min}$ are the upper and the lower bounds of the energy spectrum, respectively. $\Phi_0 = \Psi(R,r,\theta,t=0)$ is the initial real WP and $\Phi_1 = D\hat{H}_s\Phi_0$. The damping function ($D$) is applied at the grid edges along R and r coordinates.[41] The propagation was carried out by including CC between adjacent K (projection of J on body fixed z-axis) states as well as within CS approximation, where

the CCs are ignored.

The energy-dependent total reaction probability $P^r(E)$ is computed by summing the total flux passing through a fixed surface located at a sufficiently large distance (r_s) in the product channel.[42–44]

$$P^r(E) = \frac{1}{2\pi\mu_r |a_i(E)^2| (H^-)^2 \sin^2\Theta} \times \mathrm{Im}\Big\langle \sum_k (2-\delta_{k0})\, e^{-ik\Theta}\, \Phi_k \Big| \sum_{k'} (2-\delta_{k'0})\, e^{-ik'\Theta} \times \Big[\delta(r-r_s)\frac{\delta}{\delta r}\Phi_{k'}\Big]\Big\rangle, \tag{2}$$

where $\Theta = \cos^{-1}[(E-H^+)/H^-]$. Here the energy amplitude a_E is written as,[45–47]

$$a_i(E) = \Big\langle i\sqrt{\frac{\mu_R \mathbf{k}_i}{2\pi}} R h^{(2)}_{l_0}(\mathbf{k}_i R) | G_{\mathbf{k}_0}(R)\Big\rangle, \tag{3}$$

where $h^{(2)}_{l_0}$ is the spherical Hankel function of second kind and $\mathbf{k}_i = \sqrt{2\mu_R E_c}/\hbar^2$. $G_{\mathbf{k}_0}(R)$ is a real Gaussian WP, representing the translational part of the initial WP. l_0 is the initial orbital angular momentum quantum number, which lies within $|J-j_0|$ to $(J+j_0)$. In the CS calculations for $j_0 > 0$, l_0 is taken as the nearest integer root of the equation $l_0(l_0+1) = J(J+1) + j_0(j_0+1) - 2K^2$.[48] For the CC calculations, the J-dependent total reaction probabilities were calculated by averaging over all possible l_0-dependent total reaction probabilities.[46]

As CC calculations are very expensive, for (v_0, j_0) = (0,1) and (1,0), exact total reaction probabilities were calculated for all the Js less than 40 and thereafter, Js in multiple of five up to $J_{\max}$ are calculated. To calculate the probabilities for the intermediate Js, a 'J-shifting' technique[49] is applied. In this approach, probabilities for a particular J at a collision energy E_c is obtained using a linear interpolation between two known probabilities P^{J_1} (probability for J_1) and P^{J_2} (probability for J_2) as

$$\begin{aligned} P^J_{v_0,j_0}(E_c) &= P^{J_1}_{v_0,j_0}(E_c - (V^*_J - V^*_{J_1}))\frac{(J_2-J)}{(J_2-J_1)} \\ &\quad + P^{J_2}_{v_0,j_0}(E_c + (V^*_{J_2} - V^*_J))\frac{(J-J_1)}{(J_2-J_1)}. \end{aligned} \tag{4}$$

Here V_J^* is the energy threshold for the corresponding J and is calculated from[50] $V_J^* = AJ + BJ^2 + CJ^3$. The A, B and C coefficients in the above expression are obtained by fitting the threshold energies of the probabilities for the known J values.

The total integral cross section (ICS) is obtained from the J and l_0-dependent probabilities as

$$\sigma_{v_0,j_0}(E_c) = \frac{\pi}{\mathbf{k}^2_{v_0,j_0}} \sum_{J=0}^{J_{max}} \frac{(2J+1)}{(2j_0+1)} \sum_{l_0} P^J_{v_0,j_0,l_0}(E_c), \tag{5}$$

where $\mathbf{k}_{v_0,j_0}$ is the magnitude of the wave vector corresponding to the initial state at a fixed collision energy E_c.

The parameters used in the quantum mechanical (QM) calculations are tabulated in Table 1. The reaction has been studied in the collision energy range of 0.001 - 0.5 eV. In case of QM-CC calculations, a value of $K_{\max}$ = 9 was found to be sufficient to converge the reaction probabilities for larger J values. Hence $K_{\max}$ = min (9, J) were used for all the QM-CC calculations.

Statistical quantum method

The statistical approach of references[51–53] was originally designed to treat complex-forming reactions. Theoretical details of the method can be found in those original papers and on our previous study on the reverse reaction He+NeH$^+$.[37] In essence, the initial-state-selected reaction probability for a specific value of the total angular momentum J is expressed as follows:

$$P^J_{v_0,j_0}(E_c) \simeq \frac{p^J_{v_0,j_0}(E_c) \sum_{v'j'} p^J_{v'j'}(E_c)}{\sum_{v''j''} p^J_{v''j''}(E_c)}, \tag{6}$$

where $p^J_{v_0,j_0}(E_c)$ is the capture probability of complex formation from the v_0, j_0 initial state, $p^J_{v'j'}(E_c)$ is the probability of the complex to decay to all energetically accessible HeH$^+(v', j')$ final states at the collision energy E_c and the sum on the denominator runs for all open states from both reactants and products arrangements. Cross sections are then calculated via Eq. (5) and thermal rate constants are obtained with Eq. (9).

Both CS and CC approaches described in Ref.[37] have been also employed in the present study

of the Ne+HeH^+ reaction. The values of the capture radius R_{min} defining the onset of the intermediate region where the collision complex is assumed to form are 4.0 bohr for the reactant arrangement (Ne+HeH^+) and 4.4 bohr for the products (He+NeH^+). On the other hand the asymptotic region for the log derivative propagation is defined with values for R_{max} of 9.4 bohr and 10.2 bohr for reactants and products, respectively, for the higher energy range. These are almost the same choices made in our investigation on the reverse reaction, with a slight increase in the asymptotic region for Ne+HeH^+. In fact, we will discuss in next Section about the convenience of extending this value even more, up to ~ 70 bohr, when the cross sections are obtained at the lower energy regime (10^{-5} eV) required for a proper calculation of the corresponding rate constants.

At the highest energy under consideration, $E_c = 0.5$ eV, a maximum value of $v_{\max} = 3$ vibrational levels were taken into account in the calculation for the reactant arrangement and $v'_{\max} = 5$ for the product NeH^+ diatom. Up to $j_{\max} = 17$ and $j'_{\max} = 26$ rotational levels were included for the ground vibrational state of HeH^+ and NeH^+, respectively. In addition the number of partial waves at that specific value of the collision energy is $J_{\max} = 95$.

Quasiclassical trajectory calculations

The QCT method is well documented in literature.[54,55] In this method, the set of Hamilton's differential equations of motion is numerically integrated. The initial conditions are generated from a standard Monte Carlo sampling. In this work, the rovibrational energies of HeH^+ molecule have been calculated quantum mechanically by employing the Colbert-Miller method[56] and these are later used to calculate the turning points and time periods of the diatomic rovibrational states. For comparison purposes, QCT probabilities are calculated for both j_0 = 0 and 1, following the procedure in Ref.[57] For particular values of orbital angular momentum l_0 and collision energy, the impact parameter b becomes a constant and is expressed as $b = \sqrt{l_0(l_0+1)\hbar^2}/\mu_R v_{\rm rel}$, where μ_R is the reduced mass of the reactive system and $v_{\rm rel}$ is the relative velocity of the reactants. ICSs at

different collision energies are calculated as

$$\sigma_{v_0,j_0}(E_c) = \pi b_{max}^2 \frac{N_r}{N_{tot}}(E_c), \quad (7)$$

where N_r and N_{tot} are the number of reactive and total trajectories, respectively. b_{max} is the maximum value of b for a reactive trajectory for a particular collision energy and, for each particular collision energy, is calculated by running a small batch of trajectories (10000s).

All the trajectories were started at a distance of 20 bohr between the Ne atom and center of mass of the HeH^+ molecule. Trajectory calculations were stopped when the distance between Ne and H atoms exceeded 25 bohr or distance between He and H atoms exceeded 20 bohr. An integration step size of 0.05 fs was used for all the calculations, which was sufficient to conserve the total energy and angular momentum up to eight decimals. J-dependent probabilities were computed by running a batch of 20000 trajectories at each collision energy, whereas 40000 trajectories were calculated at each collision energy to determine the integral reaction cross sections. The above mentioned set of parameters was sufficient to converge the observables to within 0.5 %.

Results and Discussion

Reaction probabilities

Initial state-selected QM-CC total reaction probabilities for some selected J values are plotted as a function of collision energy in Figure 2. The barrierless pattern exhibited by the probabilities at low values of the total angular momentum, $J \sim 10$, changes as J increases and for $J > 20$ a clear threshold for the reaction due to the corresponding centrifugal barriers is manifested. The numerous existing sharp resonances for low values of J, with widths of typically about ~ 0.001 eV, may have their origin in the PES well which can trap the collision complex for a certain time. These probabilities reach values close to 1 in the low energy range and then gradually decrease with increase in collision energy. This type of behavior has been observed for other barrierless

exothermic reactions.[23,58–63] However, in the case of (v_0,j_0) = (0,0), an increasing behavior of the probabilities is noticed in the high energy regime for small Js. For J = 50, $P(E)$ become remarkably smaller and resonances are much broader.

Similar calculations have been performed for the reaction initiated from either rotationally or vibrationally excited HeH^+ and the corresponding results are shown in Figure 2. The probabilities for (v_0, j_0) = (0,1) follow a similar pattern to that of (v_0, j_0) = (0,0), i.e. very high values at lower energy region and then, a gradual decrease with energy. But for J = 0 - 20, there are significant differences in magnitudes between the probabilities for (v_0, j_0) = (0,0-1), thus showing an average reduction of the reaction for the case of excited reactants. Such an inhibition of the reactivity by rotational excitation of the reactants has been reported for many other barrierless exothermic processes before.[62,63] As shown in our previous study,[31] the minimum energy path for the reaction corresponds to a collinear or near-collinear approach of the reactants. Rotationally excited reactants disrupt this preferred orientation for the collision and as a result, reactivity decreases when the process is initiated from $HeH^+(v_0 = 0, j_0 = 1)$.

Figure 2 also shows noticeable differences with respect to the case (v_0, j_0) = (1,0), which for smaller Js, have quite different patterns than the probabilities for (v_0, j_0) = (0,0). Probabilities for vibrationally excited reactants are almost invariant, oscillating within 0.5 and 0.65, with respect to the collision energy in the whole region. The probabilities for (v_0, j_0) = (1,0) are smaller than that for (v_0, j_0) = (0,0), up to J = 50, in the low energy region, but become similar at high collision energies. Thus, the vibrational excitation of the reactant molecules reduces the reactivity of the title collision to a large extent in the low energy region.

A comparison between the total reaction probabilities for some selected Js calculated via the QM, SQM and QCT methods is presented in Figure 3. The QM results display a marked oscillatory character, although the average performed over the K states in the CC calculations smooth somehow the corresponding QM-CC probabilities. Interestingly differences between CS and CC approaches become significant as the total angular momentum becomes larger, thus suggesting that Coriolis coupled states can not be ignored within the QM framework for sufficiently high

values of J. We noticed that some QM probabilities are > 1 at the low collision energy regime, a feature also observed in the literature for barrierless exothermic reactions studied via TD WP methods.[36,58,60,61] This may result either from poor absorption of the WP by the absorbing potential at the end of the grid or from the use of finite grid. Many test runs were carried out by varying the absorption parameters and no better convergence was found for the present grid. Probably a finer grid is needed at cold and ultra cold regions for a complete convergence of the total reaction probabilities. However, it is observed that this problem has no significant effect on average quantities like ICS calculated with the correct maximum value for the corresponding $P(E)$.

The SQM results remain above the QM probabilities at the higher energy regime, thus suggesting the role played by direct mechanism on the overall dynamics of the collision at those energies. Reaction thresholds are well described in all cases, regardlessly both the initial $HeH^+(v_0, j_0)$ rovibrational state and the value of the total angular momentum J, but some deviations up to $J = 40$ are noticed when the collision energy increases. For the higher partial waves shown in Figure 3, $J = 60$ and 70, the statistical predictions decrease somehow and the comparison with the results from the other two methods (QM and QCT) improves. The overall agreement between the CS and CC approaches within the statistical treatment suggests some differences with respect to the observed deviations in the QM results as the J increases. As opposed to the case of, for instance, the $H+O_2$ reaction,[64,65] no significant features of the probabilities obtained by means of the SQM-CC seem to be lost in the SQM-CS results.

Figure 3 also shows that the total reaction probabilities calculated by means of QCT calculations successfully reproduce the average behavior of QM probabilities, for all the cases. As expected, resonance structure of the reaction probabilities could not be reproduced via classical calculations. QCT probabilities have lower thresholds than the quantum probabilities for larger Js, which may be due to the non-inclusion of the zero point energy (ZPE) correction for the products with lesser vibrational energy than that of the ground vibrational state. In the case of $v_0 = 0$, for a significant amount of reactive trajectories ($\sim 18\%$), the products NeH^+ have energies less than the ZPE. However, this is reduced to $\sim 5\%$ for $v_0 = 1$ reactant state. As it is observed, the QCT

probabilities are closer to QM-CC than the QM-CS results. In the QM-CS method, out of plane rotations of the reagent molecule are restricted, but no such approximation exists in case of QCT calculations and this may be the reason for the good agreement between the QCT and QM-CC reaction probabilities. Despite this average accord with the QM results, QCT probabilities display some discrepancies such as the case of $J = 10$ for (v_0, j_0) = (0,0) beyond 0.35 eV or reaction probabilities for J = 10 and 30 at low energies.

An estimation of the classical lifetime of the collision complexes shows that the average lifetime is 0.1 ps at low translational energies (0.005 -0.05 eV). The lifetime of the complex is defined as the time elapsed between the first time a trajectory enters the complex region and the last exit time with the condition that the sum of three internuclear distances is less than a cut-off value of 10 bohr. This result compares well with QM estimation of 0.12 ps calculated from the average width of resonances of QM-CC probabilities at low energies.

Integral Cross Sections and Rate Constants

Total ICSs for the title reaction for different initial reactant states calculated using methods described before are presented in Figure 4. To compute QM ICS for the investigated energy range, reaction probabilities were calculated up to J = 96 for v_0 = 0 and up to J = 100 for v_0 = 1, for both the QM-CS and QM-CC calculations. All the QM-CC reaction probabilities for (v_0, j_0) = (0,0) for different Js were calculated exactly, but for the excited reactant rovibrational states QM-CC probabilities beyond $J \geq 40$ only some selected values (45, 50, 55, ..., $J_{\max}$) were solved with the exact treatment. Given the smooth dependence with collision energy observed in general for reaction probabilities at such large total angular momenta, the remaining J probabilities were estimated from the known probabilities via a J-shifting method described in section II. To check the accuracy of this approach, we also computed the QM-CC reaction probabilities for (v_0, j_0) = (0,0) using the J-shifting method. The resultant ICSs are plotted along with the exact QM-CC cross sections (those calculated from exact QM-CC probabilities) in Figure 4. An excellent agreement between the interpolated and the exact cross sections for (v_0, j_0) = (0,0) (shown in inset of

Figure 4) encourage us to use the J-shifting technique for the excited rovibrational states. Cross sections calculated with all methods here employed are devoid of thresholds, and are very large at low collision energies. These ICSs decrease rapidly with increment in translational energy up to $\sim$0.25 eV, but decrease beyond that point. This behavior of cross sections is similar to other barrierless exothermic reactions.[22,36,58–63] As it is seen in Figure 4, the oscillatory structure of quantum reaction probabilities is greatly reduced in the QM ICS plots due to the partial waves-averaging effect.

For the ground rovibrational reactant state, there are no remarkable differences between the reaction cross sections obtained using different methods, except at really low collision energies. Although the QM-CS and QM-CC probabilities for (v_0, j_0) = (0,0) and (v_0, j_0) = (1,0) certainly differ at low E_c, agreement between the cross sections obtained from the QM-CC and QM-CS methods is reasonably good. It seems that CC has less effect on average quantities for $j_0 = 0$. For rotationally excited reactant state, QM-CS results underestimate the QM-CC ICSs above 0.3 eV and it is observed that both results diverge beyond this collision energy. Thus, it is clear that CC promotes the reactivity of the rotationally excited reactants. As in the case of j_0 = 0, QM-CS cross sections are slightly larger than the QM-CC ones in the very low energy region. As mentioned previously, it is always cumbersome to converge probabilities in this regime with TD WP calculations, which require very large grids, long propagation time and precise damping procedures of the WP to conclude anything about the behavior of the reaction attributes.

Figure 4 shows that QCT results successfully reproduce the overall qualitative behavior of the QM cross sections for all the reactant states, except at very low collision energies, a regime at which the QM results exhibit a maximum peak around $\sim 3 \times 10^{-3}$ eV. For the Ne+HeH$^+$$(v_0 = 1, j_0 = 0)$ collision (bottom panel of Figure 4) the QCT approach yields cross sections which slightly overestime the QM results at the lower energies ($E_c \sim 0.11$ eV). Formation and breaking of the intermediate complex may drive the reaction at low collision energies and quantum effects like resonances become important in this region. This may be the cause of apparent disagreement between QCT and QM results at low collision energies for vibrationally or rotationally excited

reactants.

The SQM cross sections reproduce fairly well the main features of the QM results for the three different $HeH^+(v_0, j_0)$ rovibrational initial states, thus suggesting the essentially complex-forming nature of the overall dynamics. SQM-CC and SQM-CS calculations yield essentially the same results, and the only apparent difference comes from the oscillations introduced in the CC cross sections (calculated at a fewer number of energies for its computational demand) by the interpolation. In particular the agreement observed between the SQM-CC and QM-CC cross sections seems to be the result of some sort of compensation introduced by the partial waves average between the overestimation of the statistical reaction probabilities for small total angular momentum and the underestimation for the larger values J. As expected, values for the exothermic title reaction are much larger than the corresponding cross sections for the endothermic reverse reaction (see Fig. 8 of Ref. [36]) with remarkably better agreement between the QM and statistical results. The SQM approach was found to fail to describe the low energy region for the He + $NeH^+ \rightarrow HeH^+$ + Ne reaction when the process is initiated from the first vibrationally excited state $(v_0, j_0) = (1,0)$. This seems not to be the case for the present reaction.

The issue of a proper description of the low collision energy regime can also be addressed within the statistical framework. Recent investigations on the $D^+ + H_2$ reaction[66–68] revealed that the value of the radius describing the asymptotic region $R_{\max}$ has to be extended up to sufficiently large distances in order to achieve the right behaviour of the cross sections. A similar test has been performed here for the present reaction and a comparison of the corresponding ICSs can be seen in Figure 5. With $R_{\max} = 9.3$ bohr the cross sections for Ne + $HeH^+(v_0 = 0, j_0 = 0) \rightarrow NeH^+$ + He reaction calculated by means of the SQM-CS approach exhibits a deviation with respect to the expected behaviour for a converged result in a logarithmic representation with respect to the collision energy around $\sim 7 \times 10^{-3}$ eV. As seen in the figure, when the asymptotic region is enlarged up to ~ 33 bohr the convergence region extends down below 10^{-3} eV. It is however necessary to make $R_{\max} \sim 67$ bohr to ensure correct cross sections for collision energies close to $\sim 10^{-5}$ eV.

QM-CC cross sections for different initial rovibrational states are compared in Figure 6. The figure shows that the cross sections for excited ro-vibrational states are different than the results for the ground state: differences are large in the low energy region and small in the high energy regime. Cross sections for (v_0, j_0) = (0,1) are smaller than (v_0, j_0) = (0,0) cross sections in the entire energy range. ICSs for (v_0, j_0) = (1,0) start being smaller than those for the reaction from the ground rovibrational state at low collision energies but become larger beyond 0.35 eV. Substantial decrease in the ICSs at low collision energies with vibrational excitation has also been observed for exothermic C+OH reaction.[69] Inhibition of reactivity due to rotational excitation is seen for many exothermic reactions,[59,62,63] which may be related to orientation effect of the reactants. Similarities among the cross sections for different initial rovibrational states in the high energy region is also common for exothermic reactions[59,62,63,69] with no barrier along their collision paths. The ICSs for a barrierless exothermic reaction can be calculated by the Langevin capture model, which expresses the ICS for a reaction between an ion and a neutral species as[70,71]

$$\sigma_{\mathrm{Lang}}(E_c) = 2\pi \left(\frac{C_4}{E_c}\right)^{1/2}, \tag{8}$$

where $C_4 = \frac{1}{2}\frac{q^2\alpha}{(4\pi\varepsilon_0)^2}$. α denotes the dipole polarizability of the neutral reactant and ε_0 is the vacuum electric constant. α for Ne atom has been calculated at CCSD(T)/aug-cc-pVQZ level numerically to be 2.60918 a.u. using the ORCA software,[72] which agrees quite well with values from literature.[73–75] The Langevin cross sections, also shown in Figure 6, are in a fairly good agreement with the QM-CC results, especially for (v_0, j_0) = (0,1) between E_c = 0.02 - 0.22 eV. It is worth mentioning at this point that a proper description of the long-range part of the potential is required to have accurate estimation of cross sections for ionic reactions. However, the long-range part of the PES used in the present set of calculations may not be accurate enough to account for the cross sections in the low energy region. This could be the reason for the deviation of QM ICSs from the Langevin behavior at the low energies. Moreover, anisotropy of the PES[31] which leads to a non-uniform variation of the potential at large R for different θ values affects the observables

and hence, the actual cross sections for this reaction may not coincide with the simple Langevin capture results.

Initial state-specific thermal rate constants ($k_{v_0,j_0}(T)$) are calculated from the initial state selected total ICSs by averaging over collision energies as[76]

$$k_{v_0,j_0}(T) = \sqrt{\frac{8k_BT}{\pi\mu_R}}\frac{1}{(k_BT)^2}\int_0^\infty E_c\, dE_c \times e^{-E_c/k_BT}\sigma_{vj}(E_c), \tag{9}$$

where k_B is the Boltzmann constant. The results estimated from QM, SQM and QCT ICSs are plotted in Figure 7. After showing a rapid early rise, the rate constants remain almost invariant with respect to temperature. There are no differences between the rate constants obtained from QM-CC exact and interpolated cross sections for (v_0, j_0) = (0,0). This finding suggests the validity of J-shifting approximation for the title reaction. In addition, no significant differences can be seen between QM-CC and QM-CS rate constants for all the cases, except at very cold regions. QCT calculations successfully reproduce the overall behavior of QM rate constants and for (v_0, j_0) = (0,0), the agreement between QM and QCT rate constants is good. For (v_0, j_0) = (1,0), QCT rate constants overestimate the QM results.

SQM rate constants are in qualitative agreement with those obtained by means of the two other theoretical approaches employed here. The accord is specially good for the reaction initiated from the rovibrational ground state of reactants and for the case for which the largest deviations are seen, that is (v_0, j_0) = (1,0), the statistical predictions are only ~ 1.2 times larger than the QM rate constants at $T = 1000$ K. Differences between the CC and CS statistical calculations are only noticeable at low values of the temperature. For this low T regime, the SQM rate constants exhibit a similar behaviour as that observed for QM results, with decreasing values of $k(T)$ as T approaches to 0 K. A recent study on the $D^+ + H_2$ reaction concluded that rate constants tend to be independent with respect to decreasing temperature when the corresponding ICS is calculated with a sufficiently large asymptotic region for a proper description at low energies.[68] As discussed before (see Figure 5), SQM cross sections were obtained with larger values of the R_{max} radius,

and the corresponding rate constants exhibited differences at the $T < 100$ K range. In particular, the $k(T)$ calculated with the ICS starting from a minimum collision energy of 10^{-5} eV and with $R_{\max}$ enlarged up to ~ 67 bohr, yielded values which were ~ 1.7 times larger at T = 10 K than those obtained from cross sections in which $R_{\max} = 9.4$ bohr. The improvement is nevertheless not dramatic since the new thermal rate constants still display a qualitatively similar behaviour as those shown in Figure 7 (see inset on top panel of the figure).

Figure 8 shows a comparison of the initial state-resolved rate constants calculated from QM-CC ICSs with the available experimental result. Figure shows that all QM rate constants follow a similar pattern, but the rate is reduced to a large extent by vibrational or rotational excitation. At 300 K, the QM-CC rate constant for (v_0, j_0) = (0,0) is 0.79 $\times 10^{-9}$ cm^3 s^{-1}, which is within the error bar of experimental rate constant measured to be $1.25 \pm 0.625 \times 10^{-9}$ cm^3 s^{-1} by Glosík et al.[38] Here it is noteworthy that the computed rate constats are Boltzmann averaged over collision energies only but not over the rovibrational energies. Quantum dynamical calculations are very expensive for $j_0 > 0$ for these type of ion-molecule reactions and hence, we report only initial state selected rate constants in this article. Rate constant for this type of barrierless exothermic reactions can be calculated using the Langevin capture model as[70,71]

$$k_{\text{Lang}}(T) = 2\pi \left(\frac{2C_4}{\mu_R} \right)^{1/2}. \tag{10}$$

As it is clear from the above expression, $k_{\text{Lang}}(T)$ is temperature independent. For the title reaction, the value of the Langevin rate constant is 0.728×10^{-9} cm^3 s^{-1} which is consistent with the usual value for this kind of processes. $k_{\text{Lang}}(T)$ is also plotted in Figure 8. Result from the simple Langevin model is also within the error bar of the experimental results and agrees quite well with the QM results: $k_{\text{Lang}}(T)$ lies in between (v_0, j_0) = (0,0) and (0,1) rate constants, closer to (0,1) rate constants than those for (0,0). At this point, we reiterate that a proper description of the long-range interactions for a ion-molecule system is necessary to calculate the rate constants at low temperatures. In addition time independent methods, more robust to describe the dynamics at such

temperature regimes, may provide an useful insight. This is beyond the scope of this article and will be examined in future studies.

Conclusions

Reactive scattering studies for the exothermic atom-molecular ion type Ne + $HeH^+(v_0, j_0) \rightarrow$ He + NeH^+ reaction have been performed via TD WP, statistical quantum methods and by means of QCT calculations. Numerous resonances seen in the QM probability curves for small Js indicate formation of an intermediate complex during reaction. Rovibrational excitation of the reactants significantly decrease the reactivity of the reaction in the low energy regime. Differences between the SQM-CC and SQM-CS reaction probabilities are relatively small when compared to QM results, except for some small Js for (v_0, j_0) = (0,0). Minor discrepancies are found between the QM-CC and QM-CS ICSs for $j_0 = 0$ reactant state at most of the investigated energies. However, for $j_0 = 1$ reactant state, CC has been found to promote the reaction. Although at high collision energies SQM probabilities for small Js are a bit different than the corresponding QM results, SQM ICSs successfully reproduce the overall behavior of QM-ICSs and in fact, SQM ICSs are in a fairly good agreement with the QM ICSs in the high energy regime. An excellent agreement found between the QCT and QM-CC results highlights QCT as an efficient method to study this reaction. Simple Langevin capture model can also describe the reaction very well. A good agreement between the experimental and theoretically calculated rate constants have been achieved in this work. It is hoped that the present theoretical study will stimulate new experimental work on this system.

Acknowledgments

This study was supported in part by a research grant from the Department of Science and Technology, New Delhi, India (DST Project No. SB/S1/PC-035/2013). We acknowledge the Center for Development of Advance Computing (CDAC), Pune for providing us the high performance com-

puting facility. TGL would like to thank support from MICINN with Grant No. FIS2011-29596-C02-01 and LBH acknowledges support from CSIC i-COOP+ Program Ref. COOPA20039.

References

(1) Zygelman, B.; Stancil, P. C.; Dalgarno, A. Stimulated Radiative Association of He and H^+. *Astrophys. J.* **1998**, *508*, 151–156.

(2) Ferrière, K. M. The interstellar environment of our galaxy. *Rev. Mod. Phys.* **2001**, *73*, 1031–1066.

(3) Lepp, S.; Stancil, P. C.; Dalgarno, A. Atomic and molecular processes in the early Universe. *J. Phys. B: At. Mol. Opt. Phys.* **2002**, *35*, R57–R80.

(4) Dalgarno, A. Introductory Lecture The growth of molecular complexity in the Universe. *Faraday Discuss.* **2006**, *133*, 9–25.

(5) Yao, Y.; Wang, Q. D. X-ray absorption spectroscopy of the multiphase interstellar medium: Oxygen and neon abundances. *Astrophys. J.* **2006**, *641*, 930–937.

(6) Barlow, M. J.; Swinyard, B. M.; Owen, P. J.; Cernicharo, J.; Gomez, H. L.; Ivison, R. J.; Krause, O.; Lim, T. L.; Matsuura, M.; Miller, S.; Olofsson, G.; Polehampton, E. T. Detection of a Noble Gas Molecular Ion, $^{36}ArH^+$, in the Crab Nebula. *Science* **2013**, *342*, 1343–1345.

(7) Bochsler, P.; Petersen, L.; Möbius, E.; Schwadron, N. A.; Wurz, P.; Scheer, J. A.; Fuselier, S. A.; McComas, D. J.; Bzowski, M.; Frisch, P. C. Estimation of the Neon/Oxygen Abundance Ratio at the Heliospheric Termination Shock and in the Local Interstellar Medium from IBEX Observations. *Astrophys. J. Suppl. Ser.* **2012**, *198*, 13.

(8) Park, J.; Kucharek, H.; Möbius, E.; Leonard, T.; Bzowski, M.; Sokół, J. M.; Kubiak, M. A.; Fuselier, S. A.; McComas, D. J. The Ne-to-O Abundance Ratio of the Interstellar Medium from IBEX-Lo Observations. *Astrophys. J.* **2014**, *795*, 97.

(9) Grandinetti, F. Gas-phase ion chemistry of the noble gases: recent advances and future perspectives. *Eur. J. Mass Spectrom.* **2011**, *17*, 423–463.

(10) Asplund, M.; Grevesse, N.;Sauval A. J.; Scott P. The Chemical Composition Of The Sun. *Annu. Rev. Astron. Astrophys.* **2009**, *47*, 481–522.

(11) Palmieri, P.; Puzzarini, C.; Aquilanti, V.; Capecchi, G.; Cavalli, S.; De Fazio, D.; Aguilar, A.; Gimenez, X.; Lucas, J. M. Ab Initio Dynamics of the He + $H_2^+ \rightarrow HeH^+$ + H Reaction: A New Potential Energy Surface and Quantum Mechanical Cross-Sections. *Mol. Phys.* **2000**, *98*, 1835–1849.

(12) Panda, A. N.; Sathyamurthy, N. Time-Dependent Quantum Mechanical Wave Packet Study of the He + H_2^+ (v, j) $\rightarrow HeH^+$ + H Reaction. *J. Chem. Phys.* **2005**, *122*, 054304.

(13) Tang, X. N.; Xu, H.; Zhang, T.; Hou, Y.; Chang, C.; Ng, C. Y.; Chiu, Y.; Dressler, R. A.; Levandier, D. J. A Pulsed-Field Ionization Photoelectron Secondary Ion Coincidence Study of the H_2^+(X, v^+ = 0-15, N^+ = 1) + He Proton Transfer Reaction. *J. Chem. Phys.* **2005**, *122*, 164301.

(14) Lv, S.-J.; Zhang, P.-Y.; Han, K.-L.; He, G.-Z. Exact Quantum Scattering Study of the Ne + H_2^+ Reaction on a New Ab Initio Potential Energy Surface. *J. Chem. Phys.* **2010**, *132*, 014303.

(15) Zhao, J.; Luo, Y. Time-Dependent Wave Packet Quantum and Quasi-Classical Trajectory Study of He + H_2^+, D_2^+ $\rightarrow HeH^+$ + H, HeD^+ + D Reaction on an Accurate FCI Potential Energy Surface. *J. Phys. Chem. A* **2012**, *116*, 2388–2393.

(16) Fazio, D. D.; Castro-Vitores, M. D.; Aguado, A.; Aquilanti, V.; Cavalli, S. The He + H_2^+ $\rightarrow HeH^+$ + H reaction: Ab initio studies of the potential energy surface, benchmark time-independent quantum dynamics in an extended energy range and comparison with experiments. *J. Chem. Phys.* **2012**, *137*, 244306.

(17) Zhang, T.; Qian, X.-M.; Tang, X. N.; Ng, C. Y.; Chiu, Y.; Levandier, D. J.; Miller, J. S.; Dressler, R. A. A State-Selected Study of the H_2^+(X, v^+ = 0-17, N^+ = 1) + Ne Proton Transfer Reaction Using the Pulsed-Field Ionization-Photoelectron-Secondary Ion Coincidence Scheme. *J. Chem. Phys.* **2003**, *119*, 10175–10185.

(18) Xiao, J.; Yang, C.-L.; Tong, X.-F.; Wang, M.-S.; Ma, X.-G. Quasi-Classical Trajectory Study of the Ne + $H_2^+ \rightarrow NeH^+$ + H Reaction Based on Global Potential Energy Surface. *J. Phys. Chem. A* **2011**, *115*, 1486–1492.

(19) Gamallo, P.; Defazio, P.; González, M. Time Dependent Quantum Dynamics Study of the Ne + $H_2^+(v_0 = 0\text{-}4,\ j_0 = 1) \rightarrow NeH^+$ + H Proton Transfer Reaction, Including the Coriolis Coupling. A System with Oscillatory Cross Sections. *J. Phys. Chem. A* **2011**, *115*, 11525–11530.

(20) Gamallo, P.; Huarte-Larrañaga, F.; González, M. Resonances in the Ne + $H_2^+ \rightarrow NeH^+$ + H Proton-Transfer Reaction. *J. Phys. Chem. A* **2013**, *117*, 5393–5400.

(21) Gamallo, P.; Martínez, R.; Sierra, J. D.; González, M. Understanding the effect of vibrational excitation in reaction dynamics: the Ne + H_2^+ ($v = 0 - 17, j = 1$) $\rightarrow NeH^+$ + H, Ne + H^+ + H proton transfer and dissociation cross sections. *Phys. Chem. Chem. Phys.* **2014**, *16*, 6641–6648.

(22) Fazio, D. D. The H + $HeH^+ \rightarrow$ He + H_2^+ reaction from the ultra-cold regime to the three-body breakup: exact quantum mechanical integral cross sections and rate constants. *Phys. Chem. Chem. Phys.* **2014**, *16*, 11662–11672.

(23) Gamallo, P.; Akpinar, S.; Defazio, P.; Petrongolo, C. Quantum Dynamics of the Reaction H(^{2}S) + $HeH^+(X^1\Sigma^+) \rightarrow H_2^+(X^2\Sigma_g^+)$ + He(^{1}S) from Cold to Hyperthermal Energies: Time-Dependent Wavepacket Study and Comparison with Time-Independent Calculations. *J. Phys. Chem. A* **2014**, *118*, 6451–6456.

(24) Kim, S. T.; Lee, J. S. Ab Initio Study of He_2H^+ and Ne_2H^+ : Accurate Structure and Energetics. *J. Chem. Phys.* **1999**, *110*, 4413–4418.

(25) Panda, A. N.; Sathyamurthy, N. Bound and Quasibound States of He_2H^+ and He_2D^+. *J. Phys. Chem. A* **2003**, *107*, 7125–7131.

(26) Liang, J.-J.; Yang, C.-L.; Wang, L.-Z.; Zhang, Q.-G. A New Analytical Potential Energy Surface for the Singlet State of He_2H^+. *J. Chem. Phys.* **2012**, *136*, 094307.

(27) Bhattacharya, S.; Panda, A. N. Time-Dependent Quantum Dynamics of the He + H^+He Reaction. *J. Phys. B: At. Mol. Opt. Phys.* **2009**, *42*, 085201.

(28) Xu, W.; Zhang, P. Accurate Study on the Quantum Dynamics of the He + HeH^+ ($X^1\Sigma^+$) Reaction on A New ab Initio Potential Energy Surface for the Lowest $1^1A'$ Electronic Singlet State. *J. Phys. Chem. A* **2013**, *117*, 1406–1412.

(29) Koner, D.; Vats, A.; Vashishta, M.; Panda, A. N. Ab Initio Electronic Structure Investigation of Protonated Mixed Rare Gas Dimers $[NeHHe]^+$, $[ArHHe]^+$ and $[ArHNe]^+$. *Comp. Theo. Chem.* **2012**, *1000*, 19 – 25.

(30) Matcha, R. L.; Pettitt, B. M.; Meier, P. F.; Pendergast, P. Potential Energy Surface for the Collinear Reaction of Ne and HeH^+. *J. Chem. Phys.* **1978**, *69*, 2264–2265.

(31) Koner, D.; Panda, A. N. Quantum Dynamical Study of the He + NeH^+ Reaction on a New Analytical Potential Energy Surface. *J. Phys. Chem. A* **2013**, *117*, 13070–13078.

(32) Guo, H. Quantum Dynamics of Complex-Forming Bimolecular Reactions. *Int. Rev. Phys. Chem.* **2012**, *31*, 1–68.

(33) Chu, T.-S.; Han, K.-L. Coriolis Coupling Effect in Molecular Reaction Dynamics. *Ann. Rep. Prog. Chem., Sect. C: Phys. Chem.* **2012**, *108*, 10–33.

(34) Chu, T.-S.; Han, K.-L. Effect of Coriolis Coupling in Chemical Reaction Dynamics. *Phys. Chem. Chem. Phys.* **2008**, *10*, 2431–2441.

(35) Hankel, M. Coriolis Coupling Effects in the Dynamics of Deep Well Reactions: Application to the $H^+ + D_2$ Reaction. *Phys. Chem. Chem. Phys.* **2011**, *13*, 7948–7960.

(36) Xu, W.; Li, W.; Lv, S.; Zhai, H.; Duan, Z.; Zhang, P. Coriolis Coupling Effects in $O^+(^4S) + H_2$ $(X^1\Sigma_g^+) \rightarrow OH^+(X^3\Sigma^-) + H(^2S)$ Reaction and Its Isotopic Variants: Exact Time-Dependent Quantum Scattering Study. *J. Phys. Chem. A* **2012**, *116*, 10882–10888.

(37) Koner, D.; Barrios, L.; González-Lezana, T.; Panda, A. N. Wave packet and statistical quantum calculations for the $He + NeH^+ \rightarrow HeH^+ + Ne$ reaction on the ground electronic state. *J. Chem. Phys.* **2014**, *141*, 114302.

(38) Glosík, J.; Twiddy, N. D.; Javahery, G.; Ferguson, E. E. Measurement of the equilibrium constant of the reaction $HeH^+ + Ne \rightleftharpoons NeH^+ + He$ in a selected ion flow tube. *Int. J. Mass Spectrom. Ion Processes* **1991**, *109*, 75–81.

(39) Zhang, J. Z. H. *Theory and Application of Quantum Molecular Dynamics*; World Scientific, 1999.

(40) Mandelshtam, V. A.; Taylor, H. S. Spectral Projection Approach to the Quantum Scattering Calculations. *J. Chem. Phys.* **1995**, *102*, 7390–7399.

(41) Sun, Z.; Lee, S.-Y.; Guo, H.; Zhang, D. H. Comparison of second-order split operator and Chebyshev propagator in wave packet based state-to-state reactive scattering calculations. *J. Chem. Phys.* **2009**, *130*, 174102.

(42) Meijer, A. J. H. M.; Goldfield, E. M.; Gray, S. K.; Balint-Kurti, G. G. Flux Analysis for Calculating Reaction Probabilities with Real Wave Packets. *Chem. Phys. Lett.* **1998**, *293*, 270–276.

(43) Lin, S. Y.; Guo, H. Quantum Wave Packet Study of Reactive and Inelastic Scattering between $C(^1D)$ and H_2. *J. Chem. Phys.* **2003**, *119*, 11602–11608.

(44) Lin, S. Y.; Sun, Z.; Guo, H.; Zhang, D. H.; Honvault, P.; Xie, D.; Lee, S.-Y. Fully Coriolis-Coupled Quantum Studies of the $H + O_2$ (v_i = 0-2, j_i = 0,1) $\rightarrow$ OH + O Reaction on an

Accurate Potential Energy Surface: Integral Cross Sections and Rate Constants. *J. Phys. Chem. A* **2008**, *112*, 602–611.

(45) Althorpe, S. C. Quantum Wavepacket Method for State-to-State Reactive Cross Sections. *J. Chem. Phys.* **2001**, *114*, 1601–1616.

(46) Lin, S. Y.; Guo, H. Quantum Wave Packet Studies of the $C(^1D) + H_2 \rightarrow CH + H$ Reaction: Integral Cross Section and Rate Constant. *J. Phys. Chem. A* **2004**, *108*, 2141–2148.

(47) Lin, S. Y.; Guo, H. Quantum state-to-state cross sections for atom-diatom reactions: A Chebyshev real wave packet approach. *Phys. Rev. A* **2006**, *74*, 022703.

(48) Lara, M.; Aguado, A.; Paniagua, M.; Roncero, O. State-to-state reaction probabilities using bond coordinates: Application to the Li+HF(v, j) collision. *J. Chem. Phys.* **2000**, *113*, 1781–1794.

(49) Miquel, I.; González, M.; Sayós, R.; Balint-Kurti, G. G.; Gray, S. K.; Goldfield, E. M. Quantum reactive scattering calculations of cross sections and rate constants for the $N(^2D) + O_2(X^3\Sigma_g^-) \rightarrow O(^3P) + NO(X\ ^2\Pi)$ reaction. *J. Chem. Phys.* **2003**, *118*, 3111–3123.

(50) Aslan, E.; Bulut, N.; Castillo, J. F.; Bañares, L.; Roncero, O.; Aoiz, F. J. Accurate Time-Dependent Wave Packet Study of the Li + H_2^+ Reaction and Its Isotopic Variants. *J. Phys. Chem. A* **2012**, *116*, 132–138.

(51) Rackham, E. J.; Huarte-Larrañaga, F.; Manolopoulos, D. E. Coupled-channel statistical theory of the $N(^2D) + H_2$ and $O(^1D) + H_2$ insertion reactions. *Chem. Phys. Lett.* **2001**, *343*, 356–364.

(52) Rackham, E. J.; González-Lezana, T.; Manolopoulos, D. E. A rigorous test of the statistical model for atom–diatom insertion reactions. *J. Chem. Phys.* **2003**, *119*, 12895–12907.

(53) González-Lezana, T. Statistical quantum studies on insertion atom-diatom reactions. *Int. Rev. Phys. Chem.* **2007**, *26*, 29–91.

(54) Truhlar, D. G.; Muckerman, J. T. In *Atom - Molecule Collision Theory*; Bernstein, R. B., Ed.; Springer US, 1979; pp 505–566.

(55) Henriksen, N. E.; Hansen, F. Y. *Theories of Molecular Reaction Dynamics*; Oxford, 2011.

(56) Colbert, D. T.; Miller, W. H. A Novel Discrete Variable Representation for Quantum Mechanical Reactive Scattering via the S-Matrix Kohn method. *J. Chem. Phys.* **1992**, *96*, 1982–1991.

(57) Aoiz, F. J.; Sáez-Rabanos, V.; Martínez-Haya, B.; González-Lezana, T. Quasiclassical Determination of Reaction Probabilities As a function of the Total Angular Momentum. *J. Chem. Phys.* **2005**, *123*, 094101.

(58) Martínez, R.; Sierra, J. D.; Gray, S. K.; González, M. Time dependent quantum dynamics study of the $O^+ + H_2(v = 0, j = 0) \rightarrow OH^+ + H$ ion-molecule reaction and isotopic variants (D_2,HD). *J. Chem. Phys.* **2006**, *125*, 164305.

(59) Bulut, N.; Castillo, J. F.; Aoiz, F. J.; Bañares, L. Real wave packet and quasiclassical trajectory studies of the $H^+ + LiH$ reaction. *Phys. Chem. Chem. Phys.* **2008**, *10*, 821–827.

(60) Sun, Z.; Zhang, C.; Lin, S.; Zheng, Y.; Meng, Q.; Bian, W. Quantum reaction dynamics of the $C(^1D) + H_2(D_2) \rightarrow CH(D) + H(D)$ on a new potential energy surface. *J. Chem. Phys.* **2013**, *139*, 014306.

(61) Hu, M.; Xu, W.; Liu, X.; Tan, R.; Li, H. Time-dependent quantum wave packet study of the $Ar + H_2^+ \rightarrow ArH^+ + H$ reaction on a new ab initio potential energy surface for the ground electronic state ($1^2A'$). *J. Chem. Phys.* **2013**, *138*, 174305.

(62) Rao, T. R.; Goswami, S.; Mahapatra, S.; Bussery-Honvault, B.; Honvault, P. Time-Dependent Quantum Wave Packet Dynamics of the C + OH Reaction on the Excited Electronic State. *J. Chem. Phys.* **2013**, *138*, 094318.

(63) Goswami, S.; Rao, T. R.; Mahapatra, S.; Bussery-Honvault, B.; Honvault, P. Time-Dependent

Quantum Wave Packet Dynamics of S + OH Reaction on Its Electronic Ground State. *J. Phys. Chem. A* **2014**, *118*, 5915–5926.

(64) Bargueño, P.; González-Lezana, T.; Larrégaray, P.; Bonnet, L.; Rayez, J.-C.; Hankel, M.; Smith, S. C.; Meijer, A. J. H. M. Study of the H + O_2 reaction by means of quantum mechanical and statistical approaches: The dynamics on two different potential energy surfaces. *J. Chem. Phys.* **2008**, *128*, 244308.

(65) Bargueño, P.; González-Lezana, T.; Larrégaray, P.; Bonnet, L.; Rayez, J. C. Time dependent wave packet and statistical calculations on the H + O_2 reaction. *Phys. Chem. Chem. Phys.* **2007**, *9*, 1127–1137.

(66) González-Lezana, T.; Honvault, P. The H^++H_2 reaction. *Int. Rev. Phys. Chem.* **2014**, *33*, 371–395.

(67) González-Lezana, T.; Honvault, P.; Scribano, Y. Dynamics of the D^+ + H_2 $\rightarrow$ HD + H^+ reaction at the low energy regime by means of a statistical quantum method. *J. Chem. Phys.* **2013**, *139*, 054301.

(68) González-Lezana, T.; Scribano, Y.; Honvault, P. The D^+ + H_2 Reaction: Differential and Integral Cross Sections at Low Energy and Rate Constants at Low Temperature. *J. Phys. Chem. A* **2014**, *118*, 6416–6424.

(69) Bulut, N.; Zanchet, A.; Honvault, P.; Bussery-Honvault, B.; Bañares, L. Time-dependent wave packet and quasiclassical trajectory study of the C(^{3}P) + OH($X^2\,\Pi$) $\rightarrow$ CO ($X^1\Sigma^+$) + H (^{2}S) reaction at the state-to-state level. *J. Chem. Phys.* **2009**, *130*, 194303.

(70) Gioumousis, G.; Stevenson, D. P. Reactions of Gaseous Molecule Ions with Gaseous Molecules. V. Theory. *J. Chem. Phys.* **1958**, *29*, 294–299.

(71) Drake, G. W. F. *Handbook of Atomic, Molecular, and Optical Physics*; Springer, 2006.

(72) Neese, F. *ORCA, An Ab Initio, DFT and Semiempirical SCF-MO Package*; Max-Planck Institute for Bioinorganic Chemistry, Mülheim a. d. Ruhr, Germany, 2010.

(73) Kumar, A.; Meath, W. J. Integrated dipole oscillator strengths and dipole properties for Ne, Ar, Kr, Xe, HF, HCl, and HBr. *Can. J. Chem.* **1985**, *63*, 1616–1630.

(74) Maroulis, G.; Thakkar, A. J. Hyperpolarizabilities and polarizabilities of neon: Discrepancy between theory and experiment. *Chem. Phys. Lett.* **1989**, *156*, 87–90.

(75) Christiansen, O.; Jørgensen, P. The Hyperpolarizability of neon revisited. *Chem. Phys. Lett.* **1993**, *207*, 367–371.

(76) Zhang, D. H.; Zhang, J. Z. H. Full-Dimensional Time-Dependent Treatment for Diatom-Diatom Reactions: The H_2 + OH reaction. *J. Chem. Phys.* **1994**, *101*, 1146–1156.

Table 1: Parameters used in the quantum dynamical calculations (All parameters are given in atomic units).

Number of R grid points	310
Number of r grid points	132
Number of angular grid points	130
R_{min}	0.2
r_{min}	0.5
δR	0.09
δr	0.13
Centre of initial wave packet	15.0
Starting points of damping along R and r	19.0, 12.59
Analysis point along r	12.46
Number of Chebyshev iterations	22000

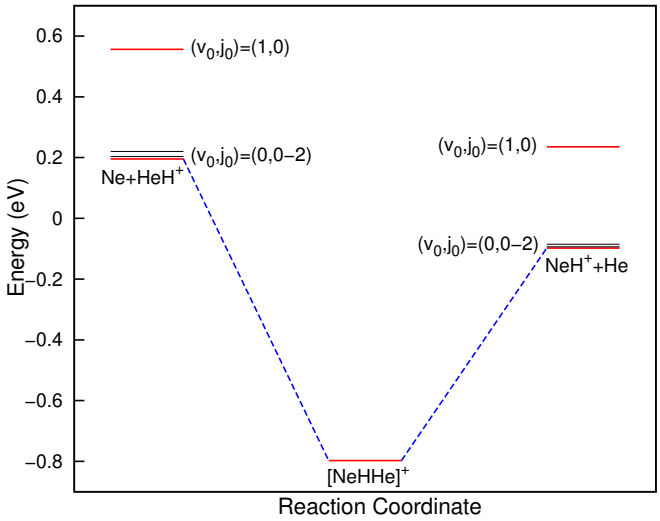

Figure 1: Schematic reaction profile of the Ne + HeH^+ $(v_0, j_0) \rightarrow NeH^+$ + He process on the ground potential energy surface. Different rovibrational states of reactants and products are also depicted.

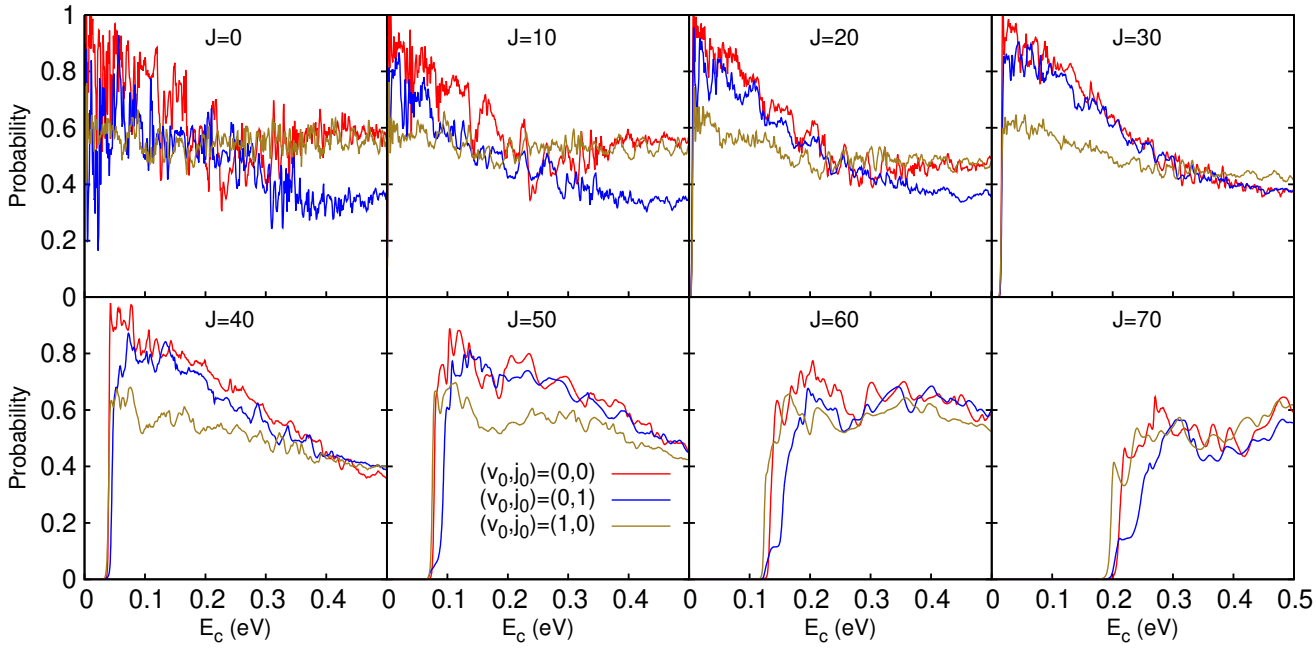

Figure 2: QM-CC total reaction probabilities for Ne + HeH^+ $(v_0, j_0) \rightarrow NeH^+$ + He for different initial reactants rovibrational states for some selected J values.

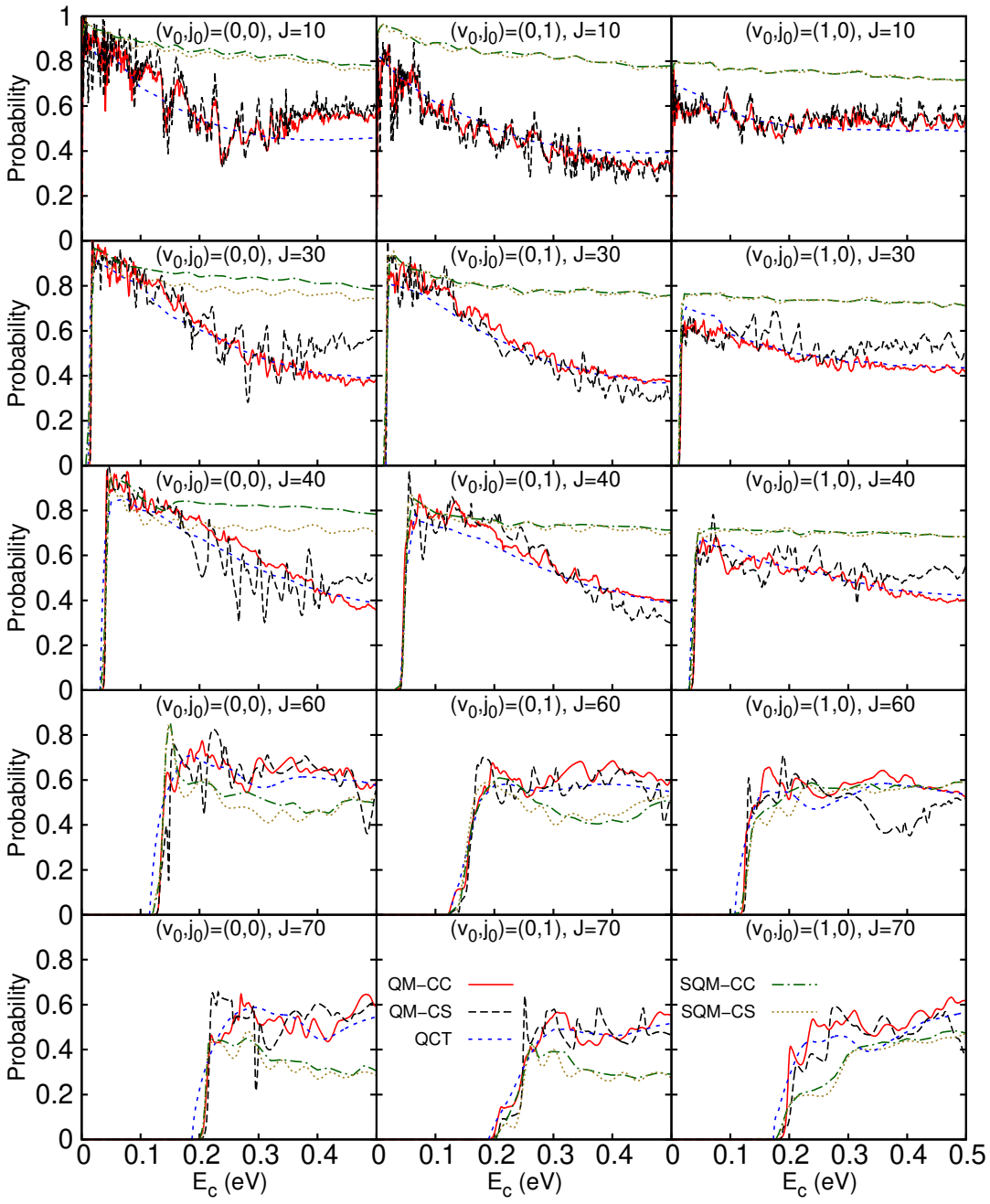

Figure 3: Total reaction probabilities as a function of collision energy for the Ne + $HeH^+(v_0, j_0) \rightarrow NeH^+$ + He reaction calculated using QM-CC, QM-CS, SQM-CC, SQM-CS and QCT methods.

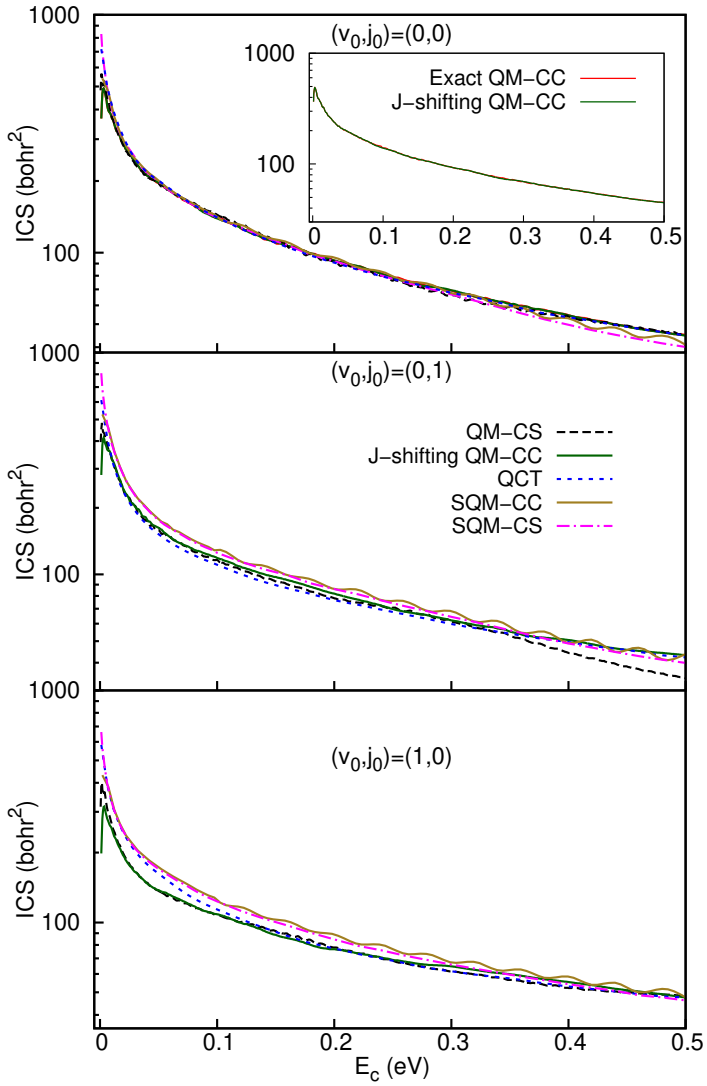

Figure 4: Total integral cross sections (ICSs) as a function of collision energy for the Ne + $HeH^+(v_0, j_0) \rightarrow NeH^+$ + He reactions obtained from quantum, statistical and classical dynamical simulations. Inset in the top panel shows a comparison between the cross sections obtained from the QM-CC exact probabilities of all the Js (red line) and those calculated from the probabilities computed via a J-shifting method (green line). Various reactant rovibrational states are indicated in the panels.

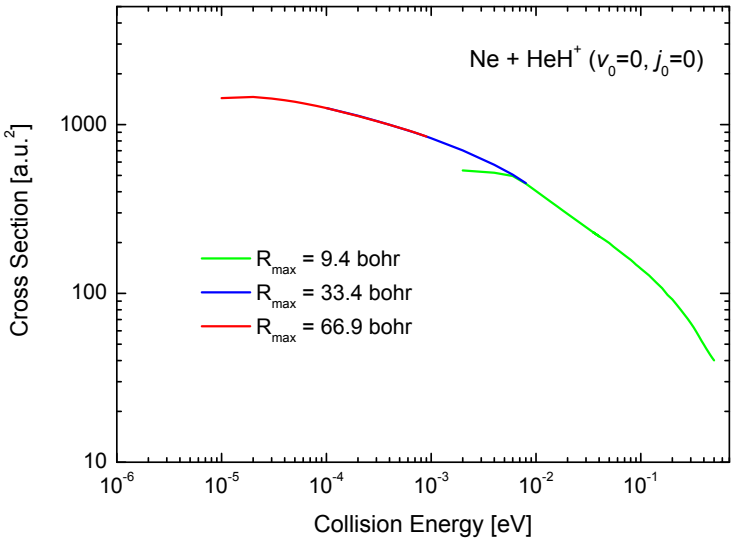

Figure 5: Cross sections for the Ne + $HeH^+(v_0 = 0, j_0 = 0) \rightarrow NeH^+$ + He reaction calculated with the SQM-CS approach with different values of the $R_{\max}$ radius. See text for details.

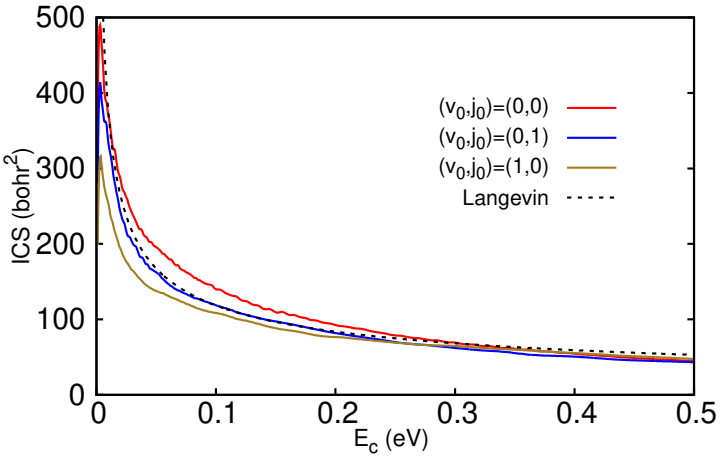

Figure 6: Comparison between QM-CC total integral cross sections for the Ne + $HeH^+(v_0, j_0)$ $\rightarrow$ NeH^+ + He reactions and the Langevin cross sections (black dashed line). QM-CC ICSs for $(v_0, j_0) = (0,1)$ and $(v_0, j_0) = (1,0)$ are calculated via a J-shifting method.

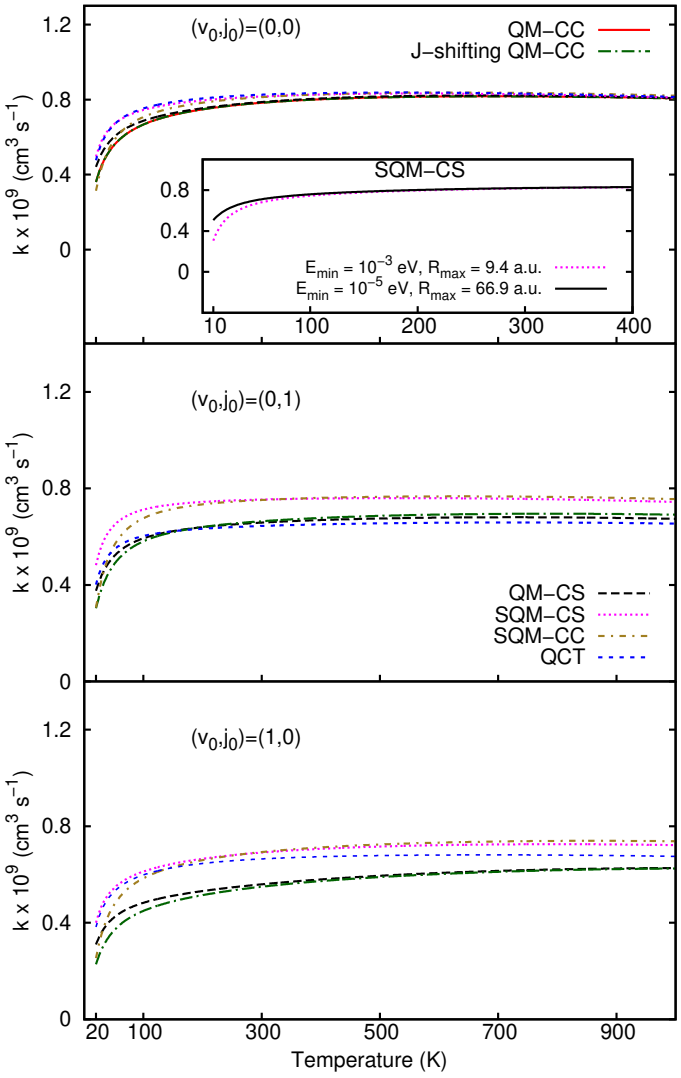

Figure 7: Temperature dependence of the rate constant for the Ne + $HeH^+(v_0, j_0) \rightarrow NeH^+$ + He reactions. Results calculated using quantum (QM-CC and QM-CS), statistical (SQM-CC and SQM-CS) and classical (QCT) cross sections are shown. The inset compares SQM-CS rate constants calculated using two different E_{min}s and the corresponding R_{max}s, for (v_0, j_0) = (0,0).

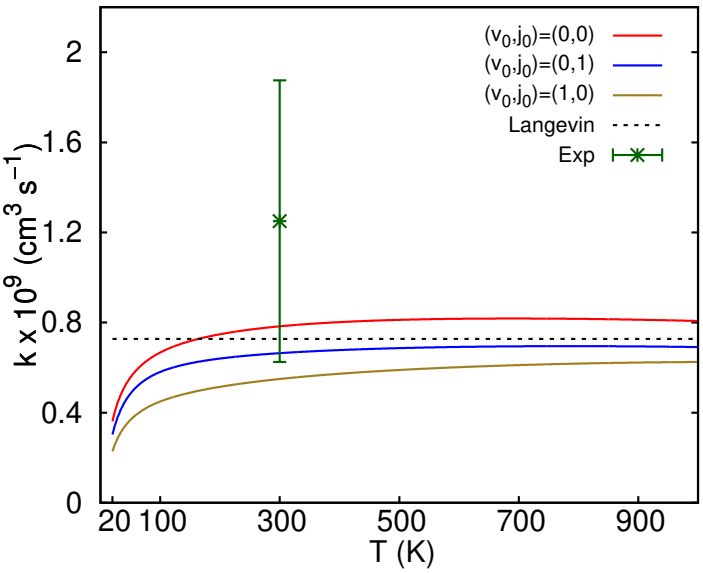

Figure 8: Comparison of state-selected QM-CC rate constants with the available experimental rate constant (green point with error bar) at 300 K[38] for the Ne + $HeH^+(v_0, j_0) \rightarrow NeH^+$ + He reactions. Rate constants calculated using the Langevin model are also shown as a black dashed line. QM-CC rate constants for $(v_0, j_0) = (0, 1)$ and $(v_0, j_0) = (1, 0)$ are calculated from the corresponding ICSs those are calculated via a J-shifting method.